Physics of the Solid State, Vol. 45, No. 12, 2003, pp. 2303–2308. Translated from Fizika Tverdogo Tela, Vol. 45, No. 12, 2003, pp. 2198–2203.

MAGNETISM AND FERROELECTRICITY

Microstructure and Properties of Co–Sm–O Nanogranular Films

G. I. Frolov, V. S. Zhigalov, S. M. Zharkov, A. I. Pol'skiĭ, and V. V. Kirgizov

Kirensky Institute of Physics, Siberian Division, Russian Academy of Sciences, Akademgorodok, Krasnoyarsk, 660036 Russia

e-mail: zharkov@iph.krasn.ru

Received April 9, 2003

Abstract—The effect of annealing on the structure and physical properties of Co–Sm–O alloy films prepared using pulsed plasma deposition is investigated. It is found that Co–Sm–O films in the initial state possess superparamagnetic properties due to the presence of small-sized magnetic nanoparticles surrounded by dielectric layers of samarium oxide in the film structure. Upon annealing, the Co–Sm–O films undergo structural transformations and exhibit a number of magnetic properties (including those inherent in both soft and hard magnetic materials). © *2003 MAIK "Nauka/Interperiodica".*

1. INTRODUCTION

In recent years, considerable research attention in materials science has been focused on the structure and properties of nanocomposites with a nanocrystalline structure. A decrease in the crystallite size in solids to a nanometric scale (1–50 nm) leads to a manifestation of a large variety of new properties that are widely used in modern technologies. The parameters of these materials are determined by both the internal properties of nanoparticles and the effects associated with the interparticle interactions. At present, magnetic alloys with a nanocrystalline structure have been extensively used to produce soft and hard magnetic materials [1, 2] and storage media for magnetic memory devices [3, 4].

The majority of soft magnetic materials with a nanocrystalline structure have been prepared through the crystallization of amorphous samples [1]. The great interest expressed by materials scientists in the study and application of soft magnetic nanomaterials stems from the unique combination of their properties, namely, the high magnetic permeability, strong magnetization, and high Curie temperature. However, the possibility of using these alloys in radio-frequency and microwave devices is limited by their high electrical conductivity. An interesting solution of this problem was proposed by Yoon *et al.* [5], who prepared Fe–Sm–O alloy films not only with good soft-magnetic properties but also with high electrical resistance owing to the specific features of the microstructure of the samples produced by magnetron sputtering.

In elaborating the above approach, we studied films prepared through pulsed plasma sputtering of an $SmCo_5$ target under vacuum (at a residual pressure of $\approx 10^{-6}$ Torr) [6]. The specific feature of this technique is the high pulsed condensation rate ($\approx 10^4$ nm/s) at a pulse duration of $\approx 10^{-4}$ s and a high cooling rate of condensates ($\approx 10^7$ K/s). Since a necessary condition for the system to attain a nanocrystalline state is rapid supercooling of the vapors, our technique is an efficient tool for preparing nanocrystalline films.

For our purpose, we prepared 50- to 75-nm-thick films on different substrates (cover glass, NaCl, amorphous sapphire). According to x-ray fluorescence analysis, the changes in the samarium content from sample to sample did not exceed 13–17 at. %. The microstructure and phase composition of the films prepared were examined using transmission electron microscopy (TEM), electron diffraction, and x-ray diffraction. Moreover, we investigated the magnetic properties (coercive force, magnetization) and electrical conductivity of the film samples. For the films deposited onto NaCl and amorphous sapphire substrates, we also studied the effect of thermal annealing (to an annealing temperature $T_{ann} \approx 780$°C) on their structure and physical properties.

Figure 1 shows typical hysteresis loops for Co–Sm–O nanocrystalline films at two temperatures. As can be seen from Fig. 1, the magnetization reversal of the Co–Sm–O film is characterized by an anhysteretic curve at room temperature and a hysteresis loop with $H_C \approx 50$ Oe at $T = 77$ K. This thermal behavior of the hysteresis loop is characteristic of superparamagnetic materials. The measured blocking temperature T_B, i.e., the temperature at which the material undergoes a transition to the superparamagnetic state, is approximately equal to 81 K. The result obtained is rather surprising, because even cobalt and iron nanocrystalline films with a grain size of smaller than 4 nm, which were prepared through either pulsed plasma deposition [6, 7] or cluster deposition [8] and whose anisotropy constant is less

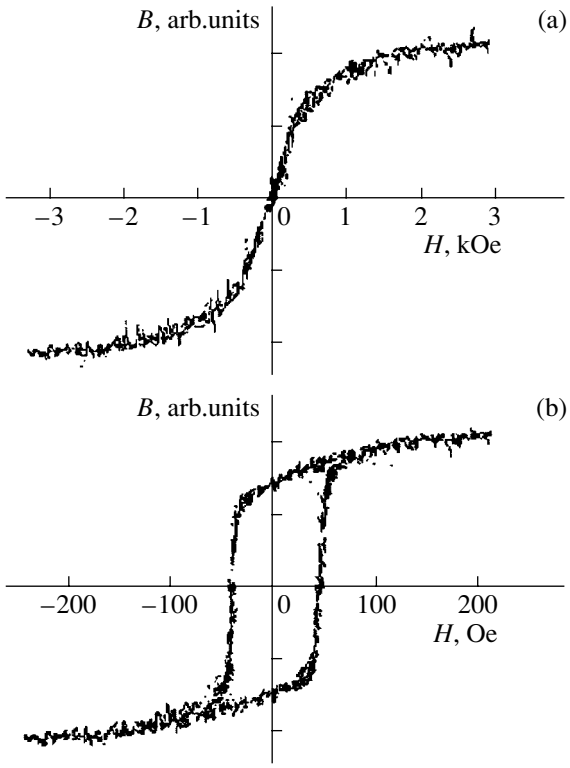

Fig. 1. Hysteresis loops for Co–Sm–O nanocrystalline films at (a) room temperature and (b) liquid-nitrogen temperature. The blocking temperature T_B is approximately equal to 81 K.

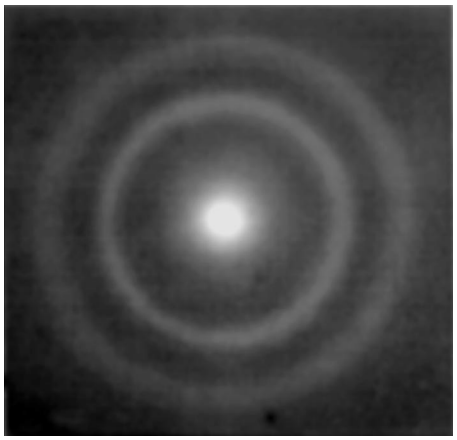

Fig. 2. Electron diffraction pattern of the Co–Sm–O film in the initial state.

than that for Sm–Co alloys, exhibit pure ferromagnetic behavior. In order to elucidate the nature of the observed effects, it was necessary to investigate the structure of the films.

2. FILM STRUCTURE IN THE INITIAL STATE

The microstructure and phase composition of the films prepared were examined using transmission electron microscopy and electron diffraction on a PRÉM-200 transmission electron microscope at an accelerating voltage of 100 kV. For these observations, a film with thickness $d \approx 50$ nm was deposited onto an NaCl substrate. Thereafter, the film was separated from the substrate in water and was then placed on a supporting grid in the electron microscope.

The electron diffraction pattern (Fig. 2) of the Co–Sm–O film in the initial state exhibits two diffuse halos of virtually identical intensity. The interplanar distances corresponding to these diffraction reflections are approximately equal to 2.97 and 2.00 Å. It seems likely that the diffraction peak centered at ≈2.97 Å can be attributed to a phase of Sm_2O_3, namely, the hexagonal modification of Sm_2O_3 (JCPDS card no. 19-1114) with the lattice parameters $a = 3.86$ Å and $c = 6.17$ Å [9]. The diffraction peak centered at ≈2.00 Å can be associated primarily with the hexagonal close-packed (hcp) or face-centered cubic (fcc) phase of cobalt and also with carbon solutions in cobalt [6, 10].

In order to obtain additional information on the original structure of the films, we performed x-ray diffraction investigations. The x-ray diffraction patterns of the films in the initial state exhibited similar reflections, and one of them was used to calculate the mean size of the crystallites. It was assumed that the broadening of the diffraction reflection observed in the x-ray diffraction pattern is caused by the size effect alone. In this case, the crystallite size can be calculated from the Scherrer formula [11]

$$\Delta 2\theta(\text{rad}) = \lambda/(D\cos\theta_0),$$

where $\Delta 2\theta$ is the half-width of the diffraction peak (rad), λ is the radiation wavelength (Å), θ_0 is the diffraction angle (deg), and D is the size of the crystallites in the sample. For the sample studied, we obtained the following diffraction parameters: $\Delta 2\theta \approx 7°$, $\theta_0 = 30°$, and $\lambda = 1.54181$ Å. As a result, we found that, for films in the initial state, the crystallite size is approximately equal to 15 Å. This indicates that the films under investigation have a nanocrystalline structure.

3. TRANSFORMATION OF THE FILM STRUCTURE UPON ANNEALING

The films placed on supporting grids were subjected to multistage annealing under a vacuum of 10^{-5} Torr, during which the films were heat treated for 30 min at each specified temperature in 25 degree intervals up to $T_{ann} = 780°C$.

According to TEM observations, the films subjected to annealing at temperatures $T_{ann} \leq 400°C$ contain dense amorphous clusters ranging in size from 0.5 to 1 μm.

However, the electron diffraction patterns of these films are identical to those of the films in the initial state (Fig. 2). Therefore, neither a change in the particle size nor a structural transformation occurs upon annealing of the films at temperatures up to and including 400°C.

After annealing at $T_{ann} > 400$°C, the electron diffraction patterns of the films exhibit diffraction spots associated with polycrystalline particles (Fig. 3a). The results of the analysis of this diffraction pattern are presented in the table. It was found that the film annealed at a temperature of 500°C contains several phases, among which the main phase is samarium oxide Sm_2O_3 with a cubic structure (JCPDS card no. 15-0813) and lattice parameter $a = 10.927$ Å [9]. The electron diffraction pattern exhibits all reflections with high and moderate intensities that are characteristic of this structure. It should be noted that this modification of samarium oxide differs from the hexagonal modification predicted for Sm_2O_3 in the Co–Sm–O film in the initial state. An analysis of the intensities of diffraction reflections $d_{hkl} = 2.063$, 1.779, 1.260, and 1.062 Å revealed the fcc cobalt phase (β-Co) and did not rule out the presence of small amounts of the hexagonal cobalt phase (α-Co, $d_{hkl} = 1.910$ and 1.149 Å) in the film. The microstructure of the film under investigation (see Fig. 3b) consists of larger sized (50–200 nm) denser clusters of samarium oxide and small-sized (10–20 nm) particles of cobalt.

Upon further annealing (up to $T_{ann} = 780$°C), no transformations of the atomic structure are observed. There only occur an increase in the number of structural clusters of samarium oxide per unit area and an insignificant increase in the cluster size (70–250 nm), whereas the size of cobalt nanoparticles remains virtually unchanged (Fig. 3c).

Therefore, we can infer that the structure of the films in the initial state consists of 1.5-nm particles of the cobalt phases separated by layers of samarium oxide. During annealing of the film, the size of cobalt particles increases to 10–20 nm and the hexagonal phase of samarium oxide undergoes a structural transformation into the cubic phase. The maximum size of Sm_2O_3 particles increases to 250 nm.

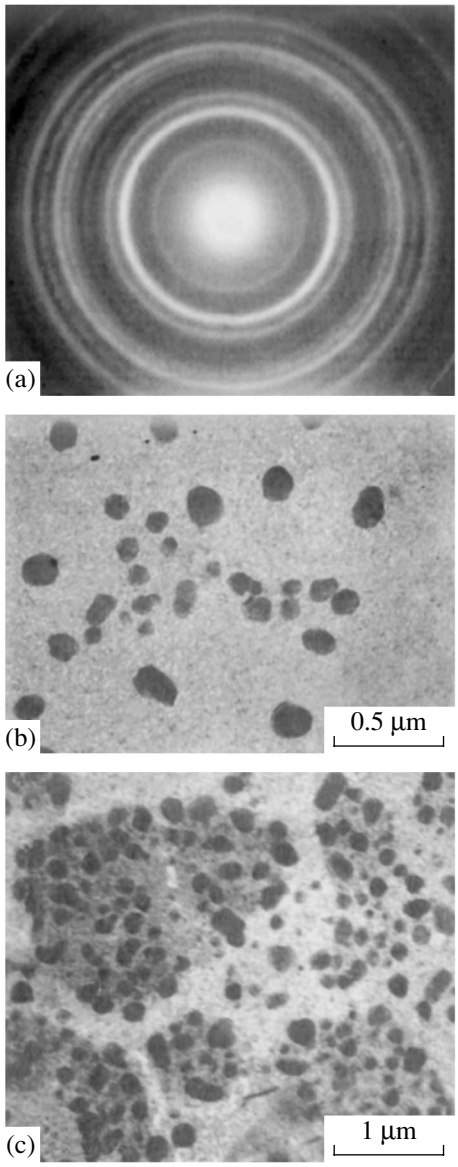

Fig. 3. Electron microscope images of Co–Sm–O films subjected to annealing at different temperatures: (a) electron diffraction pattern of the film annealed at $T_{ann} = 480$°C, (b) electron micrograph of the structure of the film annealed at $T_{ann} = 480$°C, and (c) electron micrograph of the structure of the film annealed at $T_{ann} = 700$°C.

4. EFFECT OF ANNEALING ON THE ELECTRICAL AND MAGNETIC PROPERTIES

Figure 4 shows the dependences of the electrical resistivity, the coercive force, and the saturation magnetization of the studied samples on the annealing temperature. All the measurements were performed at room temperature. The electrical resistivity ρ of the Sm–Co–O films in the initial state (Fig. 4a) is equal to 5×10^{-2} Ω cm, which is approximately four orders of magnitude greater than the values characteristic of metallic film samples ($\approx 5 \times 10^{-6}$ Ω cm) in the polycrystalline state. This confirms our assumption that metallic particles are separated by dielectric layers of samarium oxide in the film structure. An increase in the annealing temperature T_{ann} leads to an increase in the size of metallic particles, which, in turn, brings about a decrease in the electrical resistivity ρ. At an annealing temperature $T_{ann} \geq 600$°C, the electrical resistivity drastically decreases by almost three orders of magnitude as compared to that of the samples in the initial state. This can be associated with the change in the phase composition of the samples and, primarily, with the transfor-

Electron diffraction data for the Co–Sm–O film annealed under vacuum at T_{ann} = 500°C (see the electron diffraction pattern in Fig. 3a)

Co–Sm–O film (experiment)			Sm_2O_3 (JCPDS 15-0813) *la*3 a = 10.927 Å			α-Co (JCPDS 05-0727) $P6_3/mmc$ a = 2.5031 Å, c = 4.0605 Å			β-Co (JCPDS 15-0806) *Fm*3*m* a = 3.5447 Å		
No.	*d*, Å	*I*	*d*, Å	Int.	*hkl*	*d*, Å	Int.	*hkl*	*d*, Å	Int.	*hkl*
1	4.493	s	4.460	12	211						
2	3.184	vs	3.155	100	222						
3	2.750	s	2.731	35	400						
4	2.357	w	2.330	4	332						
5	2.161	w	2.143	8	431	2.165	20	100			
6	2.063	av				2.023	60	002	2.047	100	11
7	1.939	s	1.932	40	440	1.910	100	101			
8	1.779	av	1.772	6	611				1.772	40	200
9	1.656	s	1.647	30	622						
10	1.584	w	1.578	8	444						
11	1.498	w	1.487	2	721	1.480	1	102			
12	1.365	vw	1.366	4	800						
13	1.260	s	1.254	6	662	1.252	80	110	1.253	25	220
14	1.120	av	1.115	6	844	1.149	80	103			
15	1.061	av	1.071	4	1020	1.066	80	112	1.069	30	311

Note: *d* is the interplanar distance determined in the diffraction experiment, and *I* stands for the relative intensity of the diffraction reflections [the designations used for reflections are as follows: vs = very strong, s = strong, av = average, w = weak, vw = very weak]. The tabulated data for Sm_2O_3, α-Co, and β-Co are taken from [9].

mation of the microstructure, which manifests itself in the formation of large-sized particles of samarium oxide due to their rapid growth and, consequently, in the destruction of separating dielectric layers. As a result, the metallic grains form a galvanic contact.

As the annealing temperature changes, the coercive force exhibits a very complex behavior (Fig. 4b). The dependence of the coercive force of the studied samples on the annealing temperature can be divided into three portions with different values of H_C. The hysteresis loops typical of these three portions are shown in Fig. 5. The first portion of the temperature dependence of the coercive force is represented by an anhysteretic curve. This thermal behavior of the coercive force indicates that the samples are in a superparamagnetic state (Fig. 5a). The coercive force in the second portion, which lies in the annealing temperature range T_{ann} = 300–400°C, is characterized by a hysteresis loop with small values of H_C = 0.1–2 Oe (Fig. 5b). In this case, the uniaxial anisotropy field reaches H_K = 5 Oe. The appearance of the hysteresis loop can be explained by an increase in the size of cobalt nanoparticles. In the third portion ($T_{ann} \geq 400$°C), the thermal behavior of the coercive force H_C has two specific features: the coercive force first increases abruptly to 250 Oe, then decreases, and again exhibits a jump to ≈450 Oe. An analysis of the electron microscope images (Fig. 3b) revealed that, at annealing temperatures $T_{ann} \geq 400$°C, the nanocrystalline structure transforms into a polycrystalline structure and the size of cobalt nanoparticles increases by approximately one order of magnitude. As a rule, this transformation of the structure is accompanied by an increase in the coercive force H_C.

It should be noted that, as the annealing temperature increases over the entire range under investigation, the saturation magnetization J_S increases by a factor of approximately three (Fig. 4c). It seems likely that this phenomenon can be associated not only with the structural transformation but also with the phase transitions occurring in the films upon annealing. As was shown in our previous studies [6, 10, 12], which were performed with nanocrystalline cobalt films prepared according to the same technique, the film samples contain dissolved carbon in small amounts and also the metastable phases Co_3C and Co_2C, which are not ferromagnetic at room temperature. The decomposition of the carbide phases and, correspondingly, the increase in the saturation magnetization occur at the same temperatures (see [10]) at which, in our case, the saturation magnetization J_S of the films exhibits the first two features (at 250 and 400°C). In the temperature range 600–700°C, the saturation magnetization J_S undergoes a jump due to the formation of the structure consisting of a polycrystalline cobalt matrix with Sm_2O_3 inclusions. As was noted

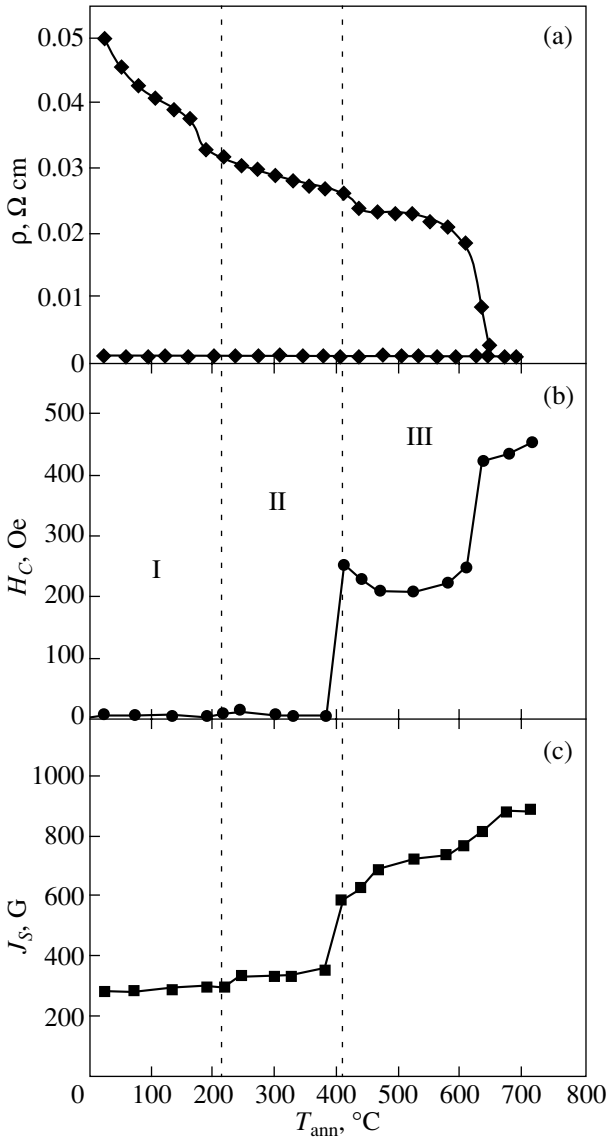

Fig. 4. Dependences of (a) the electrical resistivity, (b) the coercive force, and (c) the saturation magnetization on the annealing temperature for the Co–Sm–O film.

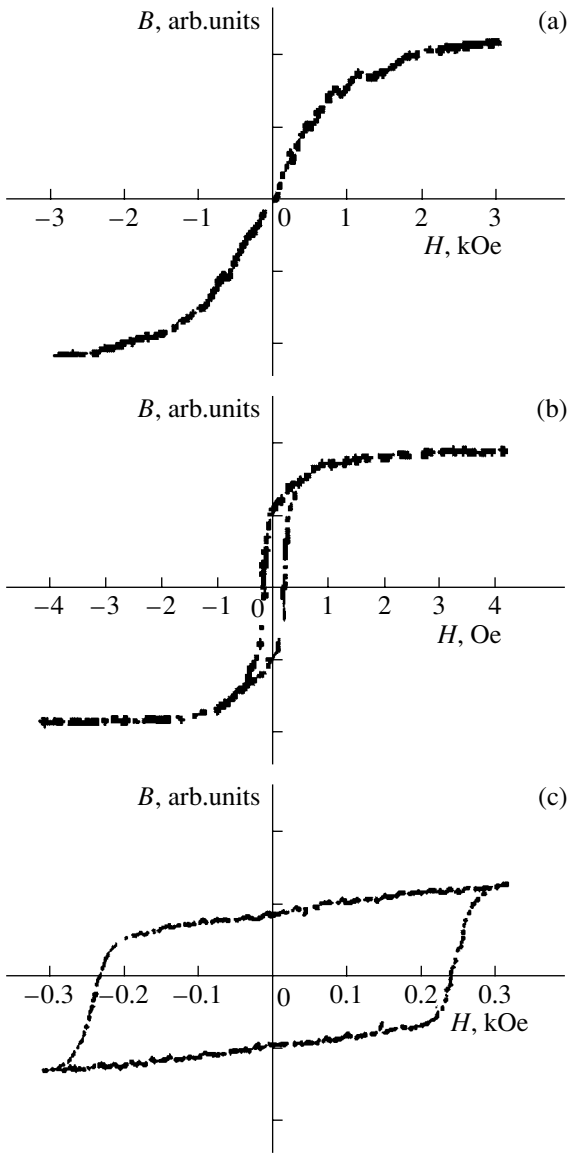

Fig. 5. Characteristic hysteresis loops for Co–Sm–O films (a) in the initial state and after annealing at (b) T_{ann} = 300°C and (c) T_{ann} = 480°C.

above, this transformation of the structure is accompanied by a number of effects: the electrical resistivity ρ drastically decreases by almost three orders of magnitude, and the coercive force H_C increases.

Let us now consider the specific features of the superparamagnetic state of the studied films prior to annealing. According to Been and Levingston [13], 3*d*-metal nanoparticles with sizes $D < 9$ nm at room temperature should be in a superparamagnetic state. However, numerous experiments have demonstrated that nanogranular films with a high content of the magnetic phase exhibit a ferromagnetic order even when the particle size is less than 5 nm [6, 8, 14, 15]. The existence of ferromagnetic order in nanogranular films can be explained both by the effects of dipole–dipole interactions between particles and by the suppression (blocking) of their magnetic state due to strong induced anisotropy. For nanogranular samples, this anisotropy is determined by a complex structure of nanoparticles with a 3*d* metal nucleus at the particle center surrounded by a passivated shell consisting of oxides or metal carbides [16, 17].

The superparamagnetic state observed in our films can be associated with a decrease in the size of nanoparticles ($D \approx 1.5$ nm), on the one hand, and with an increase in the contribution from a nonmagnetic phase (Sm_2O_3) in the bulk of grain boundaries, on the other.

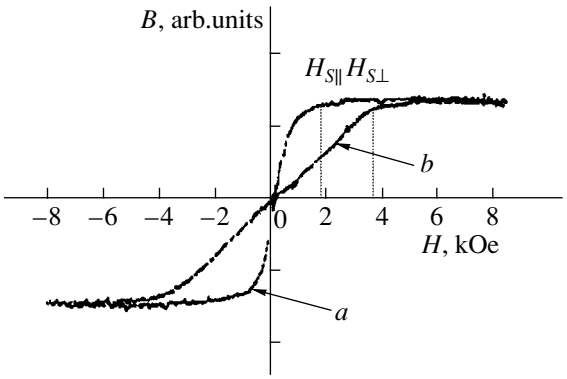

Fig. 6. Magnetization curves for a Co–Sm–O film in the initial state at $T = 300$ K in a magnetic field applied (*a*) parallel to the film plane and (*b*) perpendicular to the film plane.

As a result, the exchange interaction between nanoparticles becomes weaker.

In order to evaluate the role played by the dipole–dipole interaction, we obtained the magnetization curves for film samples at $T = 300$ K in a magnetic field applied in two directions (parallel and perpendicular to the plane of the film) (Fig. 6). As can be seen from Fig. 6, the magnetization curves are characterized by shape anisotropy. From analyzing the magnetization curves, we can assess the factors responsible for demagnetization in the plane of the film ($N_\|$) and along the normal to this plane ($N_\perp$). In a magnetic field applied perpendicular to the film plane (Fig. 6, curve *b*), the magnetization reaches saturation at a magnetic field strength $H_{S\perp} \approx 3.8$ kOe. Since the saturation magnetization of the films in the initial state is estimated as $J_S \approx 300$ G (Fig. 4c), we obtain $N_\perp = H_{S\perp}/J_S = 3.8 \times 10^3/3 \times 10^2 \approx 4\pi$ and, correspondingly, $N_\| \approx 0$. Therefore, we can state that, for our samples, the magnetic moment lies in the film plane. At the same time, the magnetization can reach saturation in the film plane only in a sufficiently strong field ($H_{S\|} \approx 1$ kOe), which suggests a strong anisotropy of disordered superparamagnetic cobalt particles.

5. CONCLUSIONS

Thus, it was found that the dependences of the electrical resistivity, the coercive force, and the saturation magnetization on the annealing temperature of Co–Sm–O films exhibit a nonmonotonic behavior. This indicates that the structural transformations of the films subjected to annealing have a complex character. However, all the structural and magnetic data obtained in this study demonstrated that no phases of $SmCo_5$ are not formed in the films studied, because the high chemical activity of samarium particles under vacuum at a residual pressure of 10^{-6} Torr leads to their oxidation.

The Co–Sm–O alloy films prepared in this work are of interest both for the study of the supermagnetism phenomenon in samples with a high content of the magnetic phase and for practical use as soft-magnetic (with a high electrical resistance) and hard-magnetic materials.

ACKNOWLEDGMENTS

This work was supported by the Russian Foundation for Basic Research (project no. 03-02-16052) and the 6th Competition of Research Projects of Young Scientists of the Russian Academy of Sciences (1999) (project no. 56).

REFERENCES

1. G. Herzer, Scr. Metall. Mater. **33** (10/11), 1741 (1995).
2. M. E. McHenry and L. E. Laughlin, Acta Mater. **1**, 223 (2000).
3. M. H. Kryder, W. Messner, and L. K. Garley, J. Appl. Phys. **79** (8), 4485 (1996).
4. G. I. Frolov, Zh. Tekh. Fiz. **71** (12), 50 (2001) [Tech. Phys. **46**, 1537 (2001)].
5. T. S. Yoon, Y. Li, W. S. Cho, and C.-O. Kim, J. Magn. Magn. Mater. **237**, 288 (2001).
6. V. S. Zhigalov, G. I. Frolov, and L. I. Kveglis, Fiz. Tverd. Tela (St. Petersburg) **40** (11), 2074 (1998) [Phys. Solid State **40**, 1878 (1998)].
7. G. I. Frolov, V. S. Zhigalov, L. I. Kveglis, *et al.*, Fiz. Met. Metalloved. **88** (2), 85 (1999).
8. J. P. Perez, V. Dupuis, J. Tuaillon, *et al.*, J. Magn. Magn. Mater. **145** (1–2), 74 (1995).
9. Powder Diffraction File, Inorganic, Card No. 15-0813 (Sm_2O_3), 19-1114 (Sm_2O_3), 05-0727 (α-Co), 15-0806 (β-Co) (JCPDS International Center for Diffraction Data, Swarthmore, PA, USA).
10. G. I. Frolov, V. S. Zhigalov, and V. K. Mal'tsev, Fiz. Tverd. Tela (St. Petersburg) **42** (2), 326 (2000) [Phys. Solid State **42**, 334 (2000)].
11. A. Guinier, *Théorie et Technique de la Radiocristallographie* (Dunod, Paris, 1956; Fizmatgiz, Moscow, 1961).
12. R. S. Iskhakov, S. V. Stolyar, L. A. Chekanova, *et al.*, Pis'ma Zh. Éksp. Teor. Fiz. **72** (6), 457 (2000) [JETP Lett. **72**, 316 (2000)].
13. C. P. Been and J. D. Levingston, J. Appl. Phys. **30**, 120S (1959).
14. J. Tuallon, V. Dupuis, P. Melionon, *et al.*, Philos. Mag. A **76**, 493 (1997).
15. G. I. Frolov, O. A. Bayukov, V. S. Zhigalov, *et al.*, Pis'ma Zh. Éksp. Teor. Fiz. **61** (1), 61 (1995) [JETP Lett. **61**, 63 (1995)].
16. J. P. Chen, C. M. Sornsen, K. J. Klabunde, and G. C. Hadjipanayis, Phys. Rev. B **51**, 11527 (1995).
17. S. T. Woods, J. R. Kirtley, Shouheng Sun, and R. H. Koch, Phys. Rev. Lett. **87**, 137205 (2001).

Translated by O. Borovik-Romanova